RJC

RASĀYAN *J. Chem.*
Vol. 15 | No. 4 |2703-2713| October - December | 2022
ISSN: 0974-1496 | e-ISSN: 0976-0083 | CODEN: RJCABP
http://www.rasayanjournal.com
http://www.rasayanjournal.co.in

TIGER-17 ANALOG ACTS AS ANANTIMICROBIAL AGENT THROUGH CELL MEMBRANE DISRUPTION: A MOLECULAR DYNAMICS SIMULATION APPROACH

G. A. Pramana[1], J. M. Dirgantara[2], M. Yusuf[1], Juliandri[1], Rustaman[1], A.T. Hidayat[1,3], U. Supratman[1,3], R. Maharani[1,3] and A. Hardianto[1,✉]

[1]Department of Chemistry, Faculty of Mathematics and Natural Sciences, Universitas Padjadjaran, Jalan Raya Bandung-Sumedang KM 21, Jatinangor, Kabupaten Sumedang, West Java 45363, Indonesia

[2]Department of Chemistry, Graduate School of Science, Osaka University, Toyonaka, Osaka 560-0043, Japan

[3]Central Laboratory, Universitas Padjadjaran, Jalan Raya Bandung-Sumedang KM 21, Jatinangor, Sumedang, West Java 45363, Indonesia

✉Corresponding Author: a.hardianto@unpad.ac.id

ABSTRACT

Tiger-17 analog, a cyclo-undodecapeptide, is a promising antimicrobial peptide (AMP). This study evaluated the potency of the tiger-17 analog as an antimicrobial agent using molecular dynamics simulation. In this work, we employed 1-palmitoyl-2-oleoyl-*sn*-glycero-3-phosphoglycerol (POPG) and zwitterionic 1-palmitoyl-2-oleoyl-*sn*-glycero-3-phosphocholine (POPC). POPG is the component of an anionic bacterial-mimicking membrane, whereas POPC represents the human cell membrane. We analyzed the membrane disruption by visualizing the snapshots and calculated some parameters, including total hydrogen bonds, area per lipid, surface accessible surface area, radial distribution functions, electron density profile, and nonbonded interaction energies. Our study suggested that the tiger-17 analog approaches the POPG membrane within 100 ns of the simulation. The peptide interacts stronger with the POPG than the POPC membrane during the simulation, supported by all analysis parameters calculated in this work. The tiger-17 analog exhibits a potential antimicrobial property with selective toxicity towards the bacterial-mimicking membrane, according to molecular dynamics simulation results. Therefore, further development of the tiger-17 analog into an antimicrobial agent is worth trying.

Keywords: Antimicrobial Peptides, Lipid Bilayer Membranes, Molecular Dynamics Simulation, Tiger-17 Analog, Cyclic Peptide.

RASĀYAN *J. Chem.*, Vol. 15, No.4, 2022

INTRODUCTION

Many antimicrobial agents are widely used for the treatment of many infectious diseases. They are massively consumed to treat various kinds of microbial infections. Antibiotics, the most general antimicrobial agent, are incredible medications to combat pathogenic microbes.[1] However, the long-term and exaggerated use of conventional antibiotics has contributed to the emersion and the spread of multi-drug-resistant microorganisms.[2] Therefore, discovering modern antimicrobials with an effective mode of action and low resistance is urgent as an alternative to conventional antimicrobials. Interestingly, antimicrobial peptides (AMPs) have the essential prerequisites to solve the quest for new antimicrobials.[3] Various AMPs were found and recorded in many databases.[4] The reported AMPs vary in their amino acid sequence, composition, and length. Some AMPs can inhibit protein biosynthesis, nucleic acid biosynthesis, protease activity, and cell division. However, in general, AMPs act as antimicrobial agents with broad-spectrum by disrupting lipid bilayer membranes of pathogenic microbes.[5-7] In the case of cell-disrupting AMPs, cationic amino acids mediate the interaction with the anionic head group of the bacterial membrane. In contrast, hydrophobic amino acids facilitate membrane association and damage. Interestingly, AMPs consist of short amino acid residues, making them economically friendly. Therefore, AMPs are applicable and promising as future antimicrobials.[8] The shortest AMP class from amphibians is tigerinins.[9] They

consist of 11-12 amino acids dominated by hydrophobic amino acids, whereas the composition of cationic amino is minor. They are characterized as AMPs with a single disulfide bridge that forms cyclic peptides with nine amino acid residues.[9,10] In 2009, Song and colleagues isolated two novel tigerinin-like AMPs from the skin secretion of crab-eating frog *Fejervaya cancrivora*, tigerinin-RC1 (RVCSAIPLPICH) and tigerinin-RC2 (RVCMAIPLPLCH). Interestingly, both AMPs exhibited broad antimicrobial spectrums.[11] subsequently, in 2014, Tang and co-workers synthesized several tigerinins-based peptides to screen wound-healing agents. They found that tiger-17, c[WCKPKPKPRCH-NH2] has the most potent wound-healing ability.[12] For the treatment of chronic and diabetic wounds, wound-healing and antimicrobial properties of the therapeutics are crucial.[13,14] Since tiger-17 comes from the tigerinins template and has primary cationic and hydrophobic residues, we expected tiger-17 to have the antimicrobial ability as well. Like tigerinins, the peptide also has a single disulfide bridge. However, such a disulfide bridge could be labile under many biological processes.[15] Therefore in the present work, we designed a tiger-17 analog, assisted by iAMPpred,[16] with head-to-tail cyclic property (c-KCWHCRPKPKP) to make the difference in the type of cyclic peptide. Nowadays, molecular dynamics simulation has become an accurate and reliable tool to investigate the behavior of lipid bilayers, including their behavior in the presence of AMPs.[17] Therefore, we undertook two 500-ns molecular dynamics simulations using the Amber20 program. The first simulation involved tiger-17 analog and human-mimicking zwitterionic membrane, 1-palmitoyl-2-oleoyl-*sn*-glycero-3-phosphocholine (POPC). The second simulation elaborated on tiger-17 analog and bacterial-mimicking anionic membrane, 1-palmitoyl-2-oleoyl-*sn*-glycero-3-phosphoglycerol (POPG).[18] We found that the tiger-17 analog interacts stronger with POPG rather than POPC.

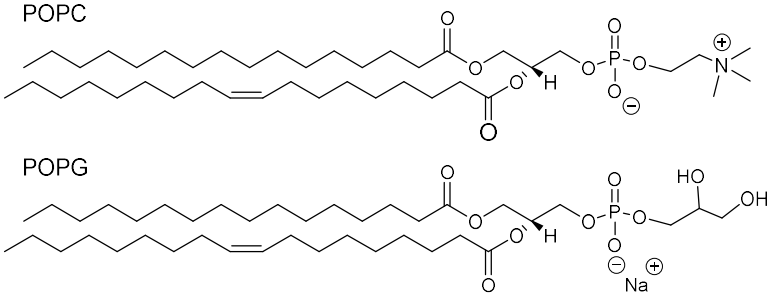

Fig.-1: Structures of POPC and POPG[1]

EXPERIMENTAL

Materials

This study was empowered by a personal computer with Intel Xeon 24 threads and NVIDIA GTX 1080Ti. Meanwhile, the software used were Amber20, Ambertools21, Biovia Discovery Studio 2019 (Dassault Systemes, Sandiego), Gaussian09, and UCSF Chimera.

Methods

iAMPpred

The iAMPpred[16] is a web server that can only predict the antimicrobial probability of linear peptides. Therefore, the linear sequence of tiger-17 analog (KCWHCRPKPKP) was submitted into the iAMPpred web server[20] in fasta format.

Modeling of Tiger-17 Analog and Membranes

On the last update of Amber20,[21] head-to-tail cyclic peptides include in their force fields. Therefore, we made the force field of tiger-17 analog a general organic molecule. A semi-empirical calculation using the PM6 method was performed using the Gaussian09 program[22] to predict the 3-dimensional structure of the fully protonated tiger-17 analog molecule. After the structural optimization of the tiger-17 analog, the partial charge of each atom of the tiger-17 analog was calculated using the hybrid functional of APFD with basis sets of D95 for hydrogen atoms and MWB2 for carbon atoms. The calculated partial charge was extracted into the Amber20 format using *antechamber*[23,24] and *parmchk2*[23] modules. The POPG and POPC lipid bilayers were built using the CHARMM-GUI membrane builder webserver.[25,26] Each lipid bilayer was settled in a periodic rectangular box with 128 molecules of lipid on the upper leaflet and 128 molecules of

lipid on the lower leaflet with 0.15 M of KCl salt in water (including counter ions of the lipid for POPG) with the Monte-Carlo positioning method. The resulting PDB file from CHARMM-GUI was reformatted by using the *tleap* tool using the *charmmlipid2amber.py* script on the AamberTools21 package.[19] On the latest update of the Amber20 program, head-to-tail cyclic peptides do not include in their force fields. Therefore, we made the force field of tiger-17 analog as a general organic molecule. A semi-empirical calculation using the PM6 basis set was performed using the Gaussian09 program[16] to predict the 3-dimensional structure of the fully protonated tiger-17 analog molecule. After the structural optimization of the tiger-17 analog, the partial charge of each atom of the tiger-17 analog was calculated with the following commands: job type (energy), basis set (genecp), functional (apfd), and method (custom). The calculated partial charge was extracted into the Amber20 format using antechamber and parmchk2 modules. A single protonated tiger-17 analog molecule in a physiological pH of 7 was placed parallel to the surface of each membrane (POPG and POPC) with a distance of 1.0 nm from the membrane's surface using the UCSF Chimera program.[27] Cl^- counter anions were added to the system. The pdb file of this system was then used for the next step of this modeling.

Molecular Dynamics Simulation Details

The molecular dynamics simulations between tiger-17 analog and lipid bilayers were prepared using the tleap tool with lipid14[28] force field for lipid molecules, gaff2[23] force field for tiger-17 analog molecule, and water.tip3p[29] for water molecules and ions. The system was minimized with positional restraint. This minimization was carried out using the steepest descent method for 300,000 cycles. These minimizations were performed in three steps with the gradual decrease of the restraint force using the *pmemd. MPI* module. The systems were then heated to 310K gradually 200 ps under the NVT (constant particle number, volume, and temperature) condition with positional restraint using the *pmemd. MPI* module. Position-restrained equilibrations were carried out with a gradual decrease of the restraint for two ns under the NVT condition using *pmemd. MPI* module, followed by equilibration for one ns under the NPT (constant particle number, pressure, and temperature) condition using *pmemd. MPI* module without restraint. Afterward, the full simulation of the systems was carried out for 500 ns without positional restraint using the *pmemd.cuda* module. The snapshots of the simulations were saved every 100 ps for the analytical requisite.

Total Hydrogen Bonds (H-bonds)

AMPs need to pass the charged lipid head groups on the penetration process through lipid bilayer membranes. These groups have high viscosity, providing abundant hydrogen bond (H-bond) networks, thus making lipid bilayers have low permeability. The strong H-bond between AMPs and the membrane indicated the deeper penetration into the membrane.[30] Therefore, total hydrogen bonds may represent membrane damage due to AMPs. In this study, we calculated the total H-bonds between tiger-17 analog and the membranes for tiger-17 analog-POPG and tiger-17 analog/POPC systems using the H-bond module in the cpptraj tool.[31]

Area per Lipid

The thickness of the membrane is spanned along the z-axis. Therefore, the area per lipid is as follows:

$$Area\ per\ lipid = \frac{L_x L_y}{N_{lipid}}$$

Where *Lx* and *Ly* are the dimensions of a membrane in *the x* and *y* axes, whereas N_{lipid} is the number of lipid molecules in one layer, calculations of area per lipid for POPC and POPG were computed using the cpptraj tool.[31]

Surface Accessible Surface Area (SASA)

In this simulation, SASA describes the accessible surface area of peptide molecule (tiger-17 analog) with solvent.[32] Tiger-17 analog SASA values were calculated using the linear combination of pairwise overlaps, which is implemented in the surf command in the cpptraj tool.[31]

Radial Distribution Function

The radial distribution function (RDF) parameter provides information regarding the frequency of certain distances.[33] A higher peak of an RDF graph indicated the more hydrogen bond formed between a set of

atoms.[30] In this work, we calculated the RDF between the head group of the membrane of each system and the tiger-17 analog using the RDF command in the cpptraj tool.[31]

Electron Density Profile

The electron density profile represents the electronic distribution of tiger-17 and phospholipid molecules along the z-axis. Electron density profiles of the two simulations were calculated using the density module in the cpptraj tool.[31]

Nonbonded Interaction Energies

Nonbonded interaction energies, including electrostatic and van der Waals terms, were computed using the NAMD Energy plugin in Visual Molecular Dynamics (VMD). The electrostatic term is expressed as follows:

$$U_{elec} = \sum_{i=1}^{n} \sum_{j>0}^{n} \frac{q_i q_j}{\varepsilon r_{ij}}$$

Where q_i and q_j are charges of two atoms and r_{ij} is the distance between them, whereas ε is the solvent dielectric constant. The term of van der Waals is represented by the Lennard-Jones (LJ) 12-6 potential:

$$U_{LJ} = \sum_{i=1}^{n} \sum_{j>0}^{n} \varepsilon_{ij} \left[\left(\frac{R_{min,i,j}}{r_{ij}} \right)^{12} - \left(\frac{R_{min,i,j}}{r_{ij}} \right)^{6} \right]$$

$R_{min,i,j}$ is the distance between two atoms at the minimum interaction energy, whereas r_{ij} is the current distance between them.

Statistical Analysis and Graphic Generation

R programming language was utilized for inferential statistical tests. Graphs were produced using a plotline library in a jupyter-notebook with a python 3.7 environment.[34] Molecular graphics were generated using VMD and Biovia Discovery Studio 2019.

RESULTS AND DISCUSSION

In this study, we investigated the potential antimicrobial activity of tiger-17 analog. As the initial prediction, we submitted the linear form of tiger-17 analog to the iAMPpred webserver. The web server generates probability ranging from 0 to 1, where a value greater than 0.5 is considered antibacterial.[14] According to the iAMPpred prediction result, the linear form of the tiger-17 analog has a probability value of 0.70-0.88, suggesting the peptide has high potency as an antimicrobial agent since the cyclic form of a peptide tends to have a higher bioactivity than its linear counterpart.[35] At the further stage, we carried out MD simulations on tiger-17 analog in the human- and bacterial-mimicking membrane models, POPC and POPG, respectively. The use of POPC was intended to study the adverse effect of tiger-17 analog to the human membrane cell. The resulting MD trajectories were analyzed into the following seven parameters: visual inspection, total hydrogen bonds, radial distribution function (RDF), area per lipid, solvent accessible surface area (SASA), electron density profiles, and nonbonded interaction energies.

Initial Visual Inspection

Figure-2 depicts the sequential snapshot representations of tiger-17 analog with different membrane models, POPC and POPG, over 500-ns MD simulations. The snapshots reveal the ability of the tiger-17 analog to interact with both membranes. Tiger-17 analog quickly approaches and interacts with both membrane surfaces on the first 100 ns. Additionally, it interacts with both membranes in distinctive conformations, changing over the simulations. For tiger-17 analog and the POPG membrane (Fig.-2, lower panel), within 100 ns, the peptide successfully approaches the phosphatidylglycerol head group of the membrane. The cationic site of the peptide initiates the interaction with the POPG membrane. Between 100 and 300 ns of the simulation, the tiger-17 analog changes its conformation to widen the contact area with the POPG membrane. In this period, the POPG membrane undergoes disruption and deformation, especially

at the binding interface with the tiger-17 analog.[36] When the membrane disruption occurs, water molecules will present across the membrane. The more considerable membrane damage will make a more significant membrane deformation and increase water molecules presented across the membrane.[17] In the rest of the simulation, the tiger-17 analog penetrates deeper into the POPG membrane and may make a hole. This hole is the track of water molecules entering the cytoplasm and disrupts the intracellular fluid to cause bacterial cell lysis.[37]

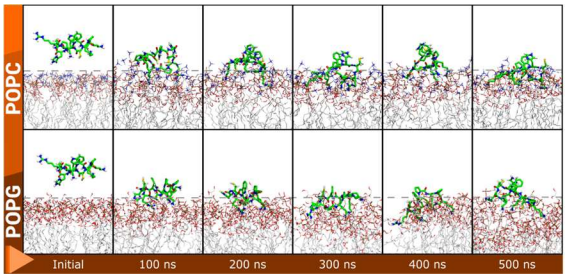

Fig.-2.: Representative Snapshots of Tiger-17 Analog in Two Different Systems, Human- and Bacterial-Mimicking Membrane Models, POPC and POPG. The carbon Atoms of Tiger-17 Analog are in Green Color, Whereas Its Nitrogen and Oxygen Atoms are in Default Colors, Blue and Red, Respectively

Tiger-17 analog also moves quickly onto the surface of the POPC membrane during the simulation. However, tiger-17 analog does not penetrate deeper into POPC than the POPG membrane. Such observation may be due to the zwitterionic property of the POPC membrane that makes the interaction between POPC and tiger-17 analog weaker than POPG and tiger-17 analog. As shown in Fig.-2, Lys and Arg residues intensively interact with POPC and POPG membranes. Cationic amino acids may play an essential role in the interaction of tiger-17 analog with both membranes. According to visual inspection (Fig.-2), positively charged residues of tiger-17 analog penetrates deeper into the membrane system of POPG than POPC. However, the selectivity of tiger-17 analog towards POPG and POPC membranes is not clear from visual inspection. Thus, in the following steps, we conducted further analyses to investigate the selectivity of tiger-17 analog towards both membranes.

Total Hydrogen Bonds between Tiger-17 Analog and Membranes

AMPs, like tiger-17 analog, need to move through the charged lipid head groups on the penetration process through lipid bilayer membranes. These groups have high viscosity, providing an extensive hydrogen bond network, thus making lipid bilayers have low permeability. The strong H-bond between AMPs and the membrane indicated the deeper penetration into the membrane.[30] Therefore, total H-bonds may represent membrane damage due to AMPs. Using the H-bond module in the cpptraj tool, we calculated the total H-bonds between tiger-17 analog and two membranes, POPC and POPG systems. The result of the H-bond analysis (Fig.-3) is consistent with the visualization inspection (Fig.-2), where the tiger-17 analog has more H-bonds with POPG than POPC, supported by a one-sided Wilcoxon rank-sum test (p-value = 1.25×10^{-7}). H-bond analysis result indicates a stronger interaction in the system of tiger-17-analog/POPG than tiger-17-analog/POPC, suggesting the peptide causes more damage to POPG than the POPC. We also found no conserved H-bond on the interaction between the tiger-17 analog and the membranes (data not shown). However, cationic residues of tiger-17 analog play a crucial role in the interaction between tiger-17 analog and both membranes.

Radial Distribution Function

Radial distribution function (RDF) was performed to investigate the passage of tiger-17 analog in the POPC and POPG membrane systems. We used phosphatidylcholine (PC) and glycero-3-phosphoglycerol (PGR) residues as POPC and POPG membrane probes, respectively. Below 15 Å, the tiger-17 analog/POPG system (Fig.-4) shows a higher RDF than the corresponding POPC system. This observation indicates that the tiger-17 analog more intensively interacts with the POPG than the POPC membrane, consistent with the total hydrogen bond calculation (Fig.-3).

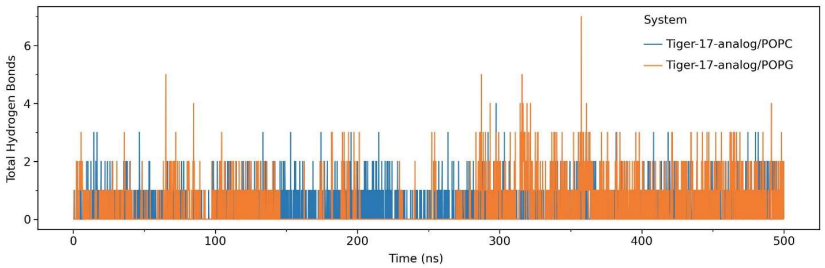

Fig.-3: Total Hydrogen Bonds Formed by Tiger-17 Analog with POPC (Blue) and POPG (Orange) Membranes in 500-Ns MD Trajectories

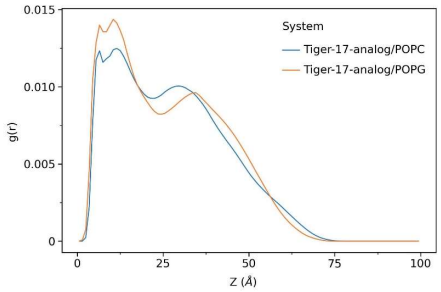

Fig.-4: Radial Distribution Function (RDF) between Tiger-17 Analog and Two Different Membrane Models, POPC (blue) and POPG (orange). The RDFs were calculated from two 500-ns MD Trajectories, Tiger-17-Analog/POPC and Tiger-17-Analog/POPG. Phosphatidylcholine (PC) and Glycero-3-Phosphoglycerol (PGR) Residues were applied as POPC and POPG Membrane Probes, respectively.

Electron Density Profiles

In this work, we also calculated the electron density profiles of POPC and POPG systems at the initial stage and the intervals of 0-100 ns and 400-500 ns as another parameter to analyze membrane damage. If the electron density plots of the tiger-17 analog and lipid bilayer overlap, the peptide penetrates the membrane. The electron density profile of the tiger-17 analog in the POPG system shifted along the z-axis during the MD simulation. This graph shows the approaching and penetrating of the tiger-17 analog to the POPG membrane (Fig.-5). The same trend also occurs for the tiger-17 analog in the POPC system. Peptide penetration depth in both systems is slightly similar (Wilcoxon rank-sum test with a *p*-value of 0.43), which may be due to the insufficient number of peptide molecules in both simulations. Nonetheless, based on our study, the damage to the membrane due to the presence of peptides could be analyzed. The trend is consistent with the data reported by Zhao and co-workers.[18]

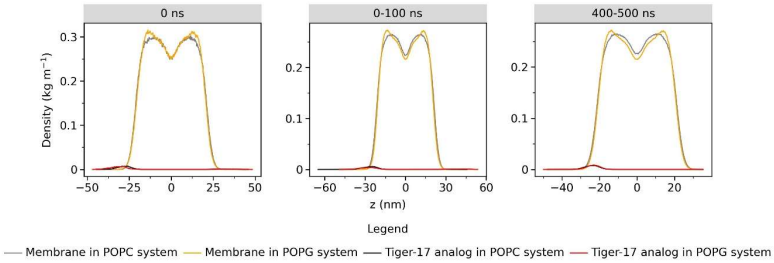

Fig.-5: Comparison of the Electron Density Profile Membranes and Tiger-17 Analog in both POPC and POPG Systems

Area per lipid

If the tiger-17 analog penetrates the membrane surface, the membrane and the peptide molecules will share the same x-y plane with one another. Such a phenomenon can be observed through the area per lipid parameter, which defines the region occupied by every lipid molecule in the membrane on the x-y plane of the MD simulation box. The lower area value per lipid indicates a higher degree of membrane damage.[38] Area per lipid plots of POPC and POPG in the presence of tiger-17 analog are presented in Fig.-6. As shown in Fig.-6, the POPG membrane has a lower area per lipid than the POPC membrane in the presence of the

tiger-17 analog. We carried out a one-sided Wilcoxon rank-sum test to confirm such a notion. The test result supports our notion that the area per lipid of the POPC membrane is significantly lower than that of the POPG membrane (p-value < 2.2×10^{-16}). Therefore, the area per lipid analysis suggests that the tiger-17 analog causes more damage to the POPG than the POPC membrane.

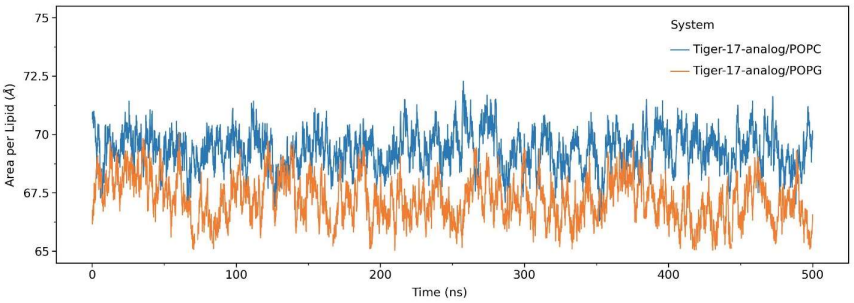

Fig.-6: Area Per Lipid of the POPC (blue) and POPG (orange) Membranes in the Presence of Tiger-17-Analog during 500 ns of MD Simulations

The first decrement started from 70 ns, which indicates the beginning interaction between the tiger-17 analog and the membrane (Fig.-8). At 70 ns of the MD trajectory, the molecular interaction between tiger-17 analog and POPG membrane was visually analyzed to characterize the membrane-interacting amino acids. This analysis (Fig.-7) found that two lysine residues and one arginine residue initialize the interaction between the peptide and POPG membrane through hydrogen bonds. This finding is consistent with the electronic property of the POPG membrane (anionic) and tiger-17 analog (cationic).

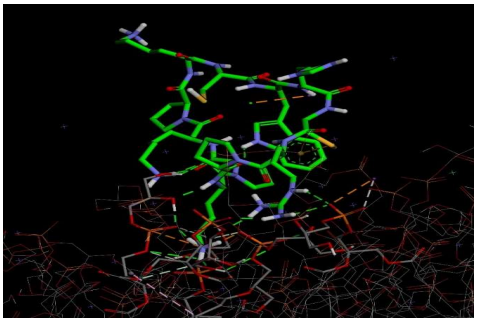

Fig.-7: Molecular Interaction between Tiger-17 Analog and POPG Membrane (t = 70 ns)

Solvent Accessible Surface Area (SASA)

Another parameter to identify membrane damage due to tiger-17 analog is solvent accessible surface area (SASA) of the peptide. If tiger-17 analog diffuses to the membrane, its SASA will decrease. Therefore, the lower SASA values of the tiger-17 analog may reflect the more severe membrane damage due to the peptide. Fig.-8 portrays SASA plots of POPC and POPG membranes in the presence of tiger-17 analog. After 200 ns of MD simulations, SASA values of tiger-17 analog tend to decrease in POPG than in the POPC membrane system. The calculated one-sided Wilcoxon rank-sum test also supports such visual inspection, where tiger-17 analog significantly has lower SASA values in the POPG than in POPC membrane system (p-value < 2.2×10^{-16}). Therefore, SASA analysis also suggests that the tiger-17 analog causes more damage to the POPG than the POPC membrane.

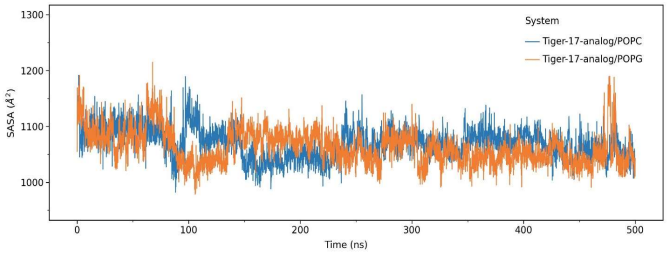

Fig.-8: SASA Profiles of Tiger-17 Analog in POPC (Blue) and POPG (Orange) Membrane Systems. SASA Values Were Calculated From 500-Ns MD Trajectories Using Cpptraj Module in Ambertools

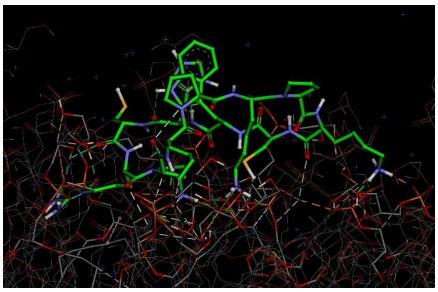

Fig.-9: Molecular Interaction between Tiger-17 Analog and POPG (t = 470 ns)

Interestingly, the SASA plot (Fig.-8) of the tiger-17 analog in the POPG system shows the same period with the area per lipid graph (Fig.-6) for the most drastic decrement. Therefore, SASA and area per lipid profiles show a consistent relationship and support each other. The decrement of SASA indicates the deeper penetration of the tiger-17 analog of each membrane. The penetrated part of the tiger-17 analog will not be accessible to the water molecules due to the different polarity between the water molecules and the tail group of lipid molecules. Interestingly, some SASA increments for the tiger-17 analog/POPG system are observed before the values drop steeply (Fig.-8). Thus, the repulsion of the tiger-17 analog by the membrane may occur. In addition, specifically within 480 ns of the simulation, there was a significant increase in the SASA. Initially, we assumed that the tiger-17 analog molecule was repulsed out of the membrane. However, the molecular interaction of the tiger-17 analog and the POPG membrane at 470 ns does not show any peptide repulsion. The peptide molecule still interacts with the POPG membrane during that period (Fig.-9). This phenomenon may be due to the water penetration into the membrane layer through the wall forms from the peptide penetration. Therefore, the SASA values of the tiger-17 analog increase significantly. By referring to the graphical trend before 480 ns of the simulation, we expected a decrease in SASA values after 500 ns of the simulation. Therefore, if we extend the duration of each simulation, POPG has more potential to penetrate the membrane deeper than we observed in this work. On the other hand, in the tiger-17 analog/POPC, the SASA of the tiger-17 analog was relatively stable after 200 ns of the simulation. Therefore, we could not expect deeper penetration of the tiger-17 analog if the simulation was extended.

Nonbonded Interactions Energies

To measure the interaction between tiger-17 analog and the membrane systems, we calculated non-bonded interaction energies, including electrostatic and van der Walls terms. The non-bonded interaction energies were calculated by using NAMD energy plugin every 100 ps of all 500-ns MD trajectories. The results (Fig.-10, left panel) clearly show that the tiger-17 analog has stronger electrostatic interactions with POPG (median -924.02 kcal/mol) than the POPC membrane (median -571.66 kcal/mol). Similarly, in Fig.-10, right panel, the peptide shows stronger van der Waals interactions with POPG (median -44.87 kcal/mol) than POPC membrane (median -35.29 kcal/mol), which also is supported by Wilcoxon rank-sum test with a *p*-value lower than 2.2×10^{-16}.

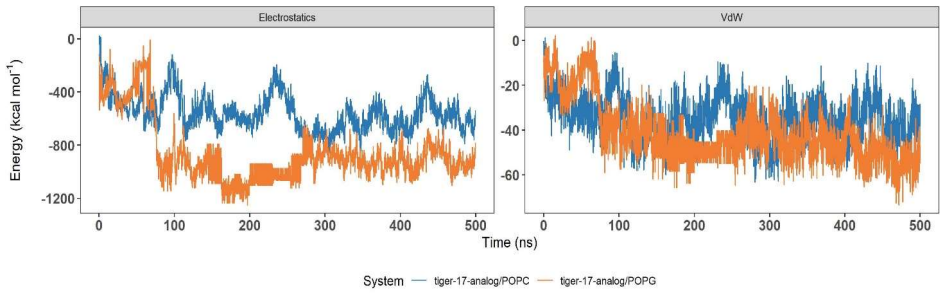

Fig.-10.: Non-Bonded Interactions Energies Between Tiger-17-Analog and Two Different Membrane Systems, POPC, and POPG Membrane. The Left Panel Shows Electrostatic Energy Profiles, Whereas the Right Panel Depicts Van Der Waals Energy Profiles

Through non-bonded interaction energies, we could clearly distinguish the binding selectivity of the tiger-17 analog. Tiger-17 analog showed a much more favorable binding energy to POPG than POPC. The ionic

interaction of tiger-17 analog cationic residues and an anionic head group of POPG is the major contributor to the binding energy of the tiger-17 analog/POPG system. Therefore, the Tiger-17 analog interacts more specifically with the POPG membrane than the POPC membrane. In the microbial-infected human body, a membrane-disrupting antimicrobial molecule will have a competitive interaction between the human membrane and microbial membrane. However, the molecule will likely interact energetically with a more favorable membrane, namely the microbial membrane.

CONCLUSION

We have conducted an *in silico* study to investigate the potential antimicrobial activity of tiger-17 analog. As the preliminary prediction, the iAMPpred webserver suggests that the linear form of tiger-17 analog has a high probability as an antimicrobial agent. In the further step, we performed detailed MD simulation analysis of tiger-17 analog in human- and bacterial-mimicking membrane models, POPC and POPG, respectively. Based on the obtained results, tiger-17 analog can be expected to have specific toxicity to the microbial membrane when applied to a microbial-infected human body even if tiger-17 analog was also able to disrupt the human-mimicking membrane, POPC. Of this fact, we have solid confidence to develop tiger-17 analog as an antimicrobial agent on a wet lab basis. Tiger-17 analog can be a promising antimicrobial molecule with strong activity and low toxicity to the human cell. Thus, the synthesis of the tiger-17 analog and its antimicrobial evaluation is the next step for developing this antimicrobial agent further.

ACKNOWLEDGEMENT

The authors would like to thank Universitas Padjadjaran and Kemdikbudristek for financial support through RDPD (1959/UN6.3.1/PT.00/2021) and PTM (094/E5/PG.02.00.PT/2022) grants, respectively.

REFERENCES

1. A. Moretta, C. Scieuzo, A.M. Petrone, R. Salvia, M.D. Manniello, A. Franco, D. Lucchetti, A. Vassallo, H. Vogel, A. Sgambato, and P. Falabella, *Frontiers in Cellular and Infection Microbiology,* **11**, 453 (2021), https://doi.org/10.3389/fcimb.2021.668632
2. H.X. Loung, T.T. Thanh, and T.H. Tran, *Life Sciences,* **260**, 118407(2020), https://doi.org/10.1016/j.lfs.2020.118407
3. M. Mahlapuu, C. Björn, and J. Ekblom, *Critical Reviews in Biotechnology*, **40(7)**, 978(2020), https://doi.org/10.1080/07388551.2020.1796576
4. G. Wang, *Pharmaceuticals*, **6(6)**, 728 (2013), https://doi.org/10.3390/ph6060728
5. K.A. Brogden, *Nature Review Microbiology*, **3(3)**, 238 (2005), https://doi.org/10.1038/nrmicro1098
6. A.T. Henriques, M.N. Melo, and M.A.R.B. Castanho, *Biochemical Journal*, **399(1)**, 1(2006), https://doi.org/10.1042/BJ20061100
7. Y. Huan, Q. Kong, H. Mou, and H. Yi, *Frontiers in Microbiology,* **11**, 582779 (2020), https://doi.org/10.3389/fmicb.2020.582779
8. S. Clark, T.A. Jowitt, L.K. Harris, C.G. Knight, and C.B. Dobson, *Communications Biology*, **4(1)**, 1(2021), https://doi.org/10.1038/s42003-021-02137-7
9. N. Sitaram, K.P. Sai, S. Singh, K. Sankaran, and R. Nagaraj, *Antimicrobial Agents and Chemotherapy,* **46(7)**, 2279 (2002), https://doi.org/10.1128/AAC.46.7.2279-2283.2002
10. K.P. Sai, M.V. Jagannadham, M. Vairamani, N.P. Raju, A.S. Devi, R. Nagaraj, and N. Sitaram, *Journal of Biologycal Chemistry*, **276(4)**, 2701 (2001), https://doi.org/10.1074/jbc.M006615200
11. Y. Song, Y. Lu, L. Wang, H. Yang, K. Zhang, and R. Lai, *Peptides,* **30(7)**, 1228 (2009), https://doi.org/10.1016/j.peptides.2009.03.020
12. J. Tang, H. Liu, C. Gao, L. Mu, S. Yang, M. Rong, Z. Zhang, J. Liu, Q. Ding, and R. Lai, *Plos One*, **9(3)**, e92082 (2014), https://doi.org/10.1371/journal.pone.0092082
13. M.L. Mangoni, A.M. McDermott, and M. Zasloff, *Experimental Dermatology,* **25(3)**, 167(2016), https://doi.org/10.1111/exd.12929
14. R.K. Thapa, D.B. Diep, and H.H. Tønnesen, *Acta Biomaterialia,* **103**, 52 (2019), https://doi.org/10.1016/j.actbio.2019.12.025

15. A.E. Pijning, J. Chiu, R.X. Yeo, J.W.H. Wong, and P.J. Hogg, *Royal Society Open Science*, **5(2)**, 171058 (2018), https://doi.org/10.1098/rsos.171058
16. P.K. Meher, T.K. Sahu, V. Saini, and A.R. Rao, *Scientific Reports*, **7(1)**, 1(2017), https://doi.org/10.1038/srep42362
17. M. Sajad, N. Amin, and S. Mohsen, *Royal Society of Chemistry Advances*, **9(8)**, 4644(2019), https://doi.org/10.1039/C8RA08441F
18. L. Zhao, Z. Cao, Y. Bian, G. Hu, J. Wang, and Y. Zhou, *International Journal of Molecular Sciences,* **19(4)**, 1186 (2018), https://doi.org/10.3390/ijms19041186
19. B. Peng, X.Y. Ding, C. Sun, Y.N. Yang, Y.J. Gao, and X. Zhao, *Royal Society of Chemistry Advances*, **7(47),** 29386 (2017), https://doi.org/10.1039/C7RA01145H
20. http://cabgrid.res.in:8080/ampred/
21. D.A. Case, H.M. Aktulga, K. Belfon, I.Y. Ben-Shalom, S.R. Brozell, D.S. Cerutti, T.E. Cheatham, III, G.A. Cisneros, V.W.D. Cruzeiro, T.A. Darden, R.E. Duke, G. Giambasu, M.K. Gilson, H. Gohlke, A.W. Goetz, R. Harris, S. Izadi, S.A. Izmailov, C. Jin, K. Kasavajhala, M.C. Kaymak, E. King, A. Kovalenko, T. Kurtzman, T.S. Lee, S. LeGrand, P. Li, C. Lin, J. Liu, T. Luchko, R. Luo, M. Machado, V. Man, M. Manathunga, K.M. Merz, Y. Miao, O. Mikhailovskii, G. Monard, H. Nguyen, K.A. O'Hearn, A. Onufriev, F. Pan, S. Pantano, R. Qi, A. Rahnamoun, D.R. Roe, A. Roitberg, C. Sagui, S. Schott-Verdugo, C.L. Simmerling, J. Shen, N.R. Skrynnikov, J. Swails, J. Smith, R.C. Walker, H. Wei, J. Wang, R.M. Wolf, X. Wu, S. Zhao, Y. Xue, D.M. York, and P.A. Kollman, Amber 2021, University of California, San Francisco, (2021).
22. Gaussian 09, A. Revision, M.J. Frisch, G.W. Trucks, H.B. Schlegel, G.E. Scuseria, M.A. Robb, J.R. Cheeseman, G. Scalmani, V. Barone, G.A. Petersson, H. Nakatsuji, X. Li, M. Caricato, A. Marenich, J. Bloino, B.G. Janesko, R. Gomperts, B. Mennucci, H.P. Hratchian, J.V. Ortiz, A.F. Izmaylov, J.L. Sonnenberg, D.W. Young, F. Ding, F. Lipparini, F. Egidi, J. Goings, B. Peng, A. Petrone, T. Henderson, D. Ranasinghe, V.G. Zakrzewski, J. Gao, N. Rega, G. Zheng, W. Liang, M. Hada, M. Ehara, K. Toyota, R. Fukuda, J. Hasegawa, M. Ishida, T. Nakajima, Y. Honda, O. Kitao, H. Nakai, T. Vreven, K. Throssell, J.A. Montgomery, Jr, F. Ogliaro, J.E. Peralta, J.J. Heyd, E. Brothers, K.N. Kudin, V.N. M. Bearpark, Staroverov, T. Keith, R. Kobayashi, S.S. Iyengar, K. Raghavachari, A. Rendell, J.C. Burant, J. Tomasi, M. Cossi, J.M. Millam, J. Normand, M. Klene, C. Adamo, R. Cammi, J.W. Ochterski, R.L. Martin, K. Morokuma, O. Farkas, J.B. Foresman, and D.J. Fox, Gaussian Inc, Wallingford CT, (2016), https://ambermd.org/AmberMD.php
23. J. Wang, W.W. Wang, P.A. Kollman, and D.A. Case, *Journal of Molecular Graphics & Modelling*, **25(2)**, 247 (2006), https://doi.org/10.1016/j.jmgm.2005.12.005
24. J. Wang, R.M. Wolf, J.W. Caldwell, P.A. Kollman, and D.A. Case, *Journal of Computational Chemistry,* **25(9)**, 1157 (2004), https://doi.org/10.1002/jcc.20035
25. S. Jo, T. Kim, V.G. Iyer, and W. Im, *Journal of Computational Chemistry,* **29(11)**, 1859(2008), https://doi.org/10.1002/jcc.20945
26. E.L. Wu, X. Cheng, S. Jo, H. Rui, K.C. Song, E.M.D. Contretas, Y. Qi, J. Lee, V.M. Galvan, R.M. Venable, J.B. Klauda, and W. Im, *Journal of Computational Chemistry,* **35(27)**, 1997(2014), https://doi.org/10.1002/jcc.23702
27. E.F. Pettersen, T.D. Goddard, C.C. Huang, G.S. Couch, D.M. Greenblatt, E.C. Meng, and T.E. Ferrin, *Journal of Computational Chemistry,* **25(13)**, 1605 (2004), https://doi.org/10.1002/jcc.20084
28. C.J. Dickson, B.D. Madej, A.A. Skjevik, R.M. Betz, K. Teigen, I.R. Gould, and R.C. Walker, *Journal of Chemical Theory and Computation*, **10(2)**, 865 (2014), https://doi.org/10.1021/ct4010307
29. W.L. Jorgensen, J. Chandrasekhar, J.D. Madura, R.W. Impey, and M.L. Klein, *Journal of Chemical Physics,* **79(2)**, 926 (1983), https://doi.org/10.1063/1.445869
30. K. Azizi, and M.G. Koli, *Journal of Molecular Graphics & Modelling*, **64**, 153(2016), https://doi.org/10.1016/j.jmgm.2016.01.009
31. D.R. Roe, and T.E. Cheatham, *Journal of Chemical Theory & Computational*, **9(7)**, 3084(2013), https://doi.org/10.1021/ct400341p
32. H. Hashemzadeh, H. Javadi, and M.H. Darvishi, *Scientific Reports*, **10(1)**, 1(2020), https://doi.org/10.1038/s41598-020-58730-z

33. X. Wu, and W. Sha, *Applied Surface Science*, **255(5)**, 2813(2008), https://doi.org/10.1016/j.apsusc.2008.08.018
34. https://plotnine.readthedocs.io/en/stable/#
35. J.T. Mika, G. Moiset, A.D. Cirac, L. Feliu, E. Bardají, M. Planas, D. Sengupta, S.J. Marrink, and B. Poolman, *Biochimica et Biophysica Acta – Biomembranes,* **180(9)**, 2197(2011), https://doi.org/10.1016/j.bbamem.2011.05.001
36. J.L.V. Bolom, G. Corzo, and R.G. Juarez, *Journal of Biomolecular Structure & Dynamics,* **36(8)**, 2070 (2018), https://doi.org/10.1080/07391102.2017.1341340
37. A. Catte, M.R. Wilson, M. Walker, and V.S. Oganesyan, *Soft Matter*, **14(15)**, 2796(2018), https://doi.org/10.1039/c7sm02152f
38. B. Zorila, G. Necula, M. Radu, and M. Bacalum, *Toxins,* **12(11)**, 705(2020), https://doi.org/10.3390/toxins12110705

[RJC-7002/2022]